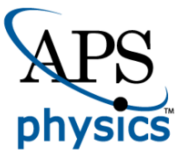

Spatial BCS-BEC crossover in superconducting p-n junctions

A. Niroula, G. Rai, S. Haas, and S. Kettemann

Phys. Rev. B **101**, 094514 — Published 23 March 2020

DOI: 10.1103/PhysRevB.101.094514

Spatial BCS-BEC crossover in superconducting p-n junctions

A. Niroula
Jacobs University, Campus Ring 1, 28759 Bremen, Germany

G. Rai
Department of Physics and Astronomy, University of Southern California, Los Angeles, CA 90089-0484, USA

S. Haas
Department of Physics and Astronomy, University of Southern California, Los Angeles, CA 90089-0484, USA and
Jacobs University, Campus Ring 1, 28759 Bremen, Germany

S. Kettemann
Jacobs University, Campus Ring 1, 28759 Bremen, Germany and
Division of Advanced Materials Science POSTECH, San 31, Hyoja-dong, Nam-gu, Pohang 790-784, South Korea
(Dated: March 5, 2020)

We present a theory of superconducting p-n junctions. To this end, we consider a two band model of doped bulk semiconductors with attractive interactions between the charge carriers and derive the superconducting order parameter, the quasiparticle density of states and the chemical potential as a function of the semiconductor gap Δ_0 and the doping level ε. We verify previous results for the quantum phase diagram for a system with constant density of states in the conduction and valence band, which show BCS-Superconductor to Bose-Einstein-Condensation (BEC) and BEC to Insulator transitions as function of doping level and the size of the band gap. Then, we extend this formalism to a density of states which is more realistic for 3D systems and derive the corresponding quantum phase diagram, where we find that a BEC phase can only exist for small band gaps $\Delta_0 < \Delta_0^*$. For larger band gaps, we find rather a direct transition from an insulator to a BCS phase. Next, we apply this theory to study the properties of superconducting p-n junctions. We derive the spatial variation of the superconducting order parameter along the p-n junction. As the potential difference across the junction leads to energy band bending, we find a spatial crossover between a BCS and BEC condensate, as the density of charge carriers changes across the p-n junction. For the 2D system, we find two possible regimes, when the bulk is in a BCS phase, a BCS-BEC-BCS junction with a single BEC layer in the space charge region, and a BCS-BEC-I-BEC-BCS junction with two layers of BEC condensates separated by an insulating layer. In 3D we find that there can also be a conventional BCS-I-BCS junction for semiconductors with band gaps exceeding Δ_0^*. Thus, we find that there can be BEC layers in the well controlled setting of doped semiconductors, where the doping level can be varied to change and control the thickness of BEC and insulator layers, making Bose Einstein Condensates thereby possibly accessible to experimental transport and optical studies in solid state materials.

PACS numbers:

I. INTRODUCTION

The existence of a superconducting state below a critical temperature T_c is not restricted to materials which are typical metals at higher temperatures, but can also occur in materials that are known to be semiconductors.[1,2] For example, superconductivity has been observed at doping concentrations as small as $4 \times 10^{17} cm^{-3}$ in $SrTiO_3$, with a critical temperature of $T_c = 0.1\,K$,[3] and in a wide range of doped semiconductors, such as B-doped diamond[4–6] and in doped silicon under high pressure,[7] with critical temperatures up to $T_c = 10\,K$.

The BCS theory of superconductivity,[8–10] can be extended and applied to such materials. Eagles[11] has solved the BCS equations within a single-band semiconductor model and found a crossover to a BEC condensate as the doping concentration is lowered. There, the charge carriers form local pairs which condense into a Bose-Einstein condensate at low temperatures.[16] Nozieres and Pistolesi[12] have extended this theory to a two-band semiconductor model and studied the superconducting-insulator transition as a function of the semiconductor energy gap, for a constant density of states in each band, as well as for a particular non constant density of states with an exponential dependence on energy. BCS-BEC crossover in multiband systems has been further studied in Refs.13,14 and15. Experimemtally, the BCS-BEC crossover has first been studied in artificial atom systems,[17].[18] Recently, the BCS-BEC has been experimentally studied in the Fe-Based superconductor $Fe_{1+y}Se_xTe_{1-x}$[19] by chemical variation of the doping level and in single-crystalline lithium-intercalated layered nitrides by gate controlled doping.[20] Superconductivity has been discovered in magic angle twisted bilayer graphene at low carrier concentrations, which is tunable by gate controled doping[21] and might open another venue to study the BCS-BEC crossover experimentally.

Junctions between p- and n-doped semiconductors form the basic element of semiconductor devices whose rectifying behavior is based on the energy band bending and on the different majority charge carriers, holes and electrons, respectively on either side of the junction. As superconductivity has been observed both in p- and n-doped semiconductors, intriguing

questions arise about the physical properties of superconducting p-n junctions[23]: how does the superconducting order parameter vary spatially across the junction? Does a p-n junction form a Josephson contact, and how large is the supercurrent across the p-n junction? Such questions have been explored for $YBa_2Cu_3O_7/Nd_{1-x}Ce_xCu_2O_4$ junctions,[22] with an estimated depletion width of less than $1\,nm$,[23] for the p-type superconductor YBa2Cu3O (YBCO) over the n-type superconducting cuprate Pr2CexCuO4 (PCCO),[25] as well as for iron pnictide p-n junctions, where the redistribution of charges could possibly lead to the suppression of the local superconducting order parameter near the interface for both single crystals. This may play a role in the junction formation itself.[24] The superconductivity in magic angle twisted bilayer graphene has been obtained both for electronic and hole gate controlled doping,[21] which might allow to form superconducting p-n junctions from twisted bilayer graphene.

Here, we study superconducting p-n junctions within a two-band model, based on a self-consistent solution of the BCS equations, the Poisson equation and the particle number conservation. In the next section, we first review the two-band theory of superconductivity for a constant density of states. Then, we generalize it to a more realistic three-dimensional density of states. We derive the pairing amplitude, the chemical potential, the quasiparticle density of states and the coherence length ξ as functions of the semiconductor band gap Δ_0 and the doping level ε. We identify the crossover between superconductivity (SC) and Bose-Einstein condensation (BEC) and derive the corresponding phase diagram in the ε-Δ_0 parameter space. Based on this model, in section III we derive the properties of a superconducting p-n-junction homojunction (with same parent material on both sides of the junction), in particular the spatial dependence of the order parameter, the quasiparticle excitation energy and the pairing coherence length across the p-n junction.

II. TWO-BAND THEORY OF SUPERCONDUCTIVITY

In order to derive the superconducting order parameter Δ and the chemical potential μ, we need to solve the BCS self-consistency equation along with the equation for the conservation of particle number N. The particle number conservation at $T = 0$ gives[12]:

$$2\int d\xi_k \rho(\xi_k) v_k^2 = N = 2\int^{\varepsilon_F} d\xi_k \rho(\xi_k), \tag{1}$$

where $\rho(\xi_k)$ is the density of states, $v_k^2 = (1-(\xi_k-\mu)/E(\xi_k))/2$ with electron energy dispersion ξ_k, $E(\xi_k) = \sqrt{(\xi_k-\mu)^2+\Delta^2}$ is the quasiparticle energy. ε_F is the Fermi energy at $T = 0K$. At $T = 0$, there are no thermally excited charge carriers. Doping introduces additional electrons or holes. However, in the dilute doping limit, electrons and holes are trapped at low temperature by the donor and acceptor atoms, respectively. As the concentration of donor atoms N_D or acceptor atoms N_A increases, their eigenstates hybridize and eventually delocalize into impurity bands, which at larger doping concentrations merge with the conduction or valence band, respectively. Here, we model the doping in a simplified way by a continuous variation of the Fermi energy, for donor doping by $\varepsilon_F = E_C + \varepsilon_n$ and for acceptor doping by $\varepsilon_F = E_V - \varepsilon_p$ (see Fig. 1).

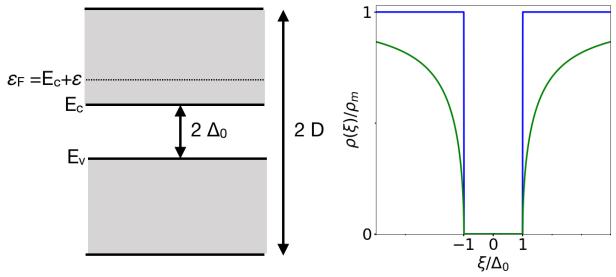

FIG. 1: Left: two-band model with valence band edge $E_V = -\Delta_0$, and conduction band edge $E_C = \Delta_0$, semiconductor band gap $2\Delta_0$, total band width $2D$. Energy range with attractive pairing $2\omega_D$ around Fermi energy $\varepsilon_F = E_c + \varepsilon$ with doping level ε. Right: model densities of states as a function of energy: 2D DOS (blue) and 3D DOS (green).

These doping parameters are related to the donor concentration N_D and the acceptor concentration N_A, respectively, for the 2D DOS via $N_D = 2\rho_0\varepsilon_n, N_A = 2\rho_0\varepsilon_p$, where the factor 2 accounts for the spin degeneracy. For the 3D DOS, one finds $N_D = 2\frac{2}{3}\rho_0\,\varepsilon_n^{\frac{3}{2}}, N_A = 2\frac{2}{3}\rho_0\,\varepsilon_p^{\frac{3}{2}}$.

The BCS weak coupling theory gives for $T = 0K$ the self-consistency equation for the order parameter Δ,

$$1 = \frac{U}{2}\int_{\mu-\omega_D}^{\mu+\omega_D} d\xi_k \frac{\rho(\xi_k)}{\sqrt{(\xi_k-\mu)^2+\Delta^2}}, \tag{2}$$

where U is the attractive interaction strength, and $2\omega_D$ is the size of the typical energy window around the chemical potential μ where the effective interaction is attractive.

Quasiparticle density of states. The quasiparticle density of states is defined by

$$N(E) = -\frac{1}{\pi} Tr Im\hat{G}_E, \tag{3}$$

where E is the quasiparticle excitation energy relative to the chemical potential μ, and $\hat{G}_E$ is the quasiparticle propagator.

Noting that in the presence of the pairing gap Δ, the propagator is given by[28] $G_E(\xi_k) = (E+i\delta+\xi_k-\mu))/((E+i\delta)^2-\Delta^2-(\xi_k-\mu)^2)$, and thus we get via complex integration

$$N(E) = Re[\rho(\mu+\sqrt{E^2-\Delta^2})\frac{|E|}{\sqrt{E^2-\Delta^2}}]. \tag{4}$$

When the chemical potential is within a band, e.g. in the conduction band, $\Delta_0 < \mu < D$, the quasiparticle density of states $N(E)$ diverges at $E = \pm\Delta$, the coherence peak, and is zero for smaller energies, so that Δ is the quasiparticle gap (see Fig. 2(top) and (center)). Remarkably, in the case when the chemical potential is in the

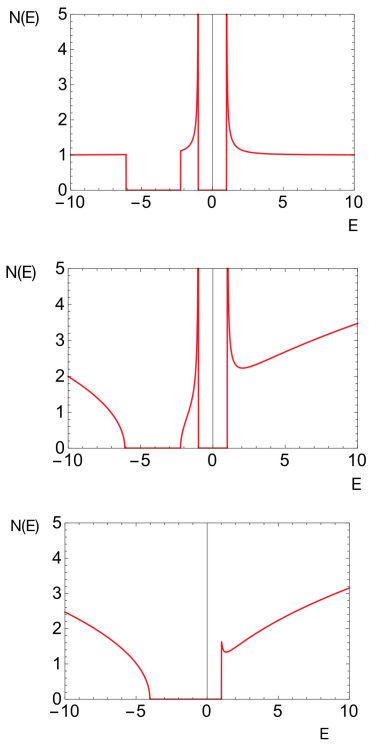

FIG. 2: 2D (Top) and 3D (Center) quasiparticle density of states, Eq. (4), as a function of quasiparticle energy E, when the chemical potential is in the conduction band. (Bottom) quasiparticle density of states as function of quasiparticle energy E for the 3D DOS, when the chemical potential is in the semiconductor band gap.

semiconductor gap, $-\Delta_0 < \mu < \Delta_0$, the quasiparticle density of states $N(E)$ does not diverge for any E, see Fig. 2(bottom) , but it is still peaked. This is an indication that the system is in a Bose-Einstein condensate, as we discuss below. Moreover, the quasiparticle gap is then enhanced to $\tilde{\Delta} = \sqrt{\Delta^2 + (\Delta_0 - |\mu|)^2} > \Delta$ exceeding the pairing order parameter Δ.

BCS-BEC Crossover. There is a crossover from BCS superconductivity to Bose-Einstein condensation (BEC) as the concentration of charges carriers is lowered by decreasing the doping level ε.[12] Let us study this BCS-BEC crossover in more detail. One way to distinguish between BCS and BEC is to measure the coherence length ξ of the condensate pairs. When $\xi > \lambda_F$, where λ_F is the Fermi wave length, many electron pairs overlap with each other, which is typical for a superconducting condensate. When $\xi < \lambda_F$, however, the electron pairs do not overlap, but they instead form well-defined bosons which condense below the transition temperature T_c. Therefore, let us next calculate ξ in the two-band model. ξ can be derived by calculating the expectation value of the distance between two electrons with opposite spin in the ground state

$$\xi^2 = \int dr r^2 g(r) / \int dr g(r). \tag{5}$$

Here, $g(r)$ is the pair correlation function in the ground state, defined by

$$g(r) = |\langle\psi|\psi_+^\dagger(r)\psi_-^\dagger(0)|\psi\rangle|^2, \tag{6}$$

where $|\psi\rangle$ is the BCS trial ground state given by

$$|\psi\rangle = \prod_k \left(u_k + v_k c_{k+}^\dagger c_{k-}^\dagger\right)|0\rangle. \tag{7}$$

Here $c_{k\alpha}^+$ are the fermion creation operators in a state with momentum k and spin $\alpha = \pm$. $|0\rangle$ is the vacuum state, and $2u_k v_k = \Delta/\sqrt{(\xi_k - \mu)^2 + \Delta^2}$. The electron field operators are given by $\psi_\alpha^+(r) = \sum_k e^{ikr} c_{k\alpha}^+$. Thereby we find

$$\xi^2 = -\sum_k u_k v_k \nabla_k^2 u_k v_k / \sum_k u_k^2 v_k^2. \tag{8}$$

We will calculate ξ below for the two-band model explicitly.

A. Two-band model with 2D DOS

Let us first review the theory for the two-band model with a constant density of states ρ in both the valence and the conduction band, separated by an energy gap $2\Delta_0$ as shown in Fig.1. This corresponds to a two-dimensional system, as considered in Ref.12. As we will mostly be interested to understand the BCS-BEC crossover limit where the Fermi energy relative to the band edge is small, we will first follow Ref.12 in assuming that ω_D is a large energy scale. This means that we assume that the electron-electron interaction is attractive in both bands, so that we can set $\omega_D = D$. Thereby, the BCS self-consistency equation simplifies to

$$1 = \frac{\rho U}{2}\left(\int_{\Delta_0}^{\omega_D} + \int_{-\omega_D}^{-\Delta_0}\right) d\xi_k \frac{1}{\sqrt{(\xi_k - \mu)^2 + \Delta^2}}, \tag{9}$$

which gives

$$\frac{2}{\rho U} = \ln\left(\frac{\omega_D - \mu + \sqrt{(\omega_D - \mu)^2 + \Delta^2}}{\Delta_0 - \mu + \sqrt{(\Delta_0 - \mu)^2 + \Delta^2}} \cdot \frac{-\Delta_0 - \mu + \sqrt{(-\Delta_0 - \mu)^2 + \Delta^2}}{-\omega_D - \mu + \sqrt{(-\omega_D - \mu)^2 + \Delta^2}}\right). \tag{10}$$

For the limiting case of a gapless, metallic system, i.e., $\Delta_0 = 0$, we can express the interaction factor ρU in terms of the superconducting order parameter Δ_m via

$$\Delta_m \equiv \Delta(\Delta_0 = 0) = 2\omega_D \exp\left(\frac{-1}{\rho U}\right), \tag{11}$$

and rewrite Eq. (10) as

$$\Delta_m^2 = \left[(\Delta_0 - \mu) + \sqrt{(\Delta_0 - \mu)^2 + \Delta^2}\right] \cdot \left[(\Delta_0 + \mu) + \sqrt{(\Delta_0 + \mu)^2 + \Delta^2}\right]. \tag{12}$$

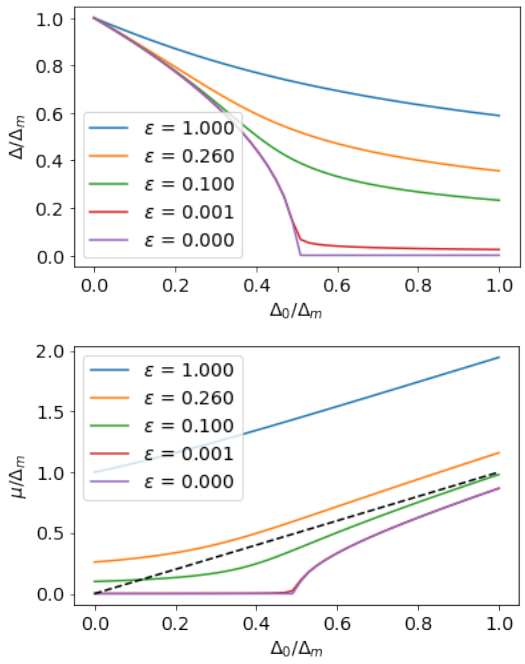

FIG. 3: Top: superconducting order parameter Δ, Bottom: chemical potential μ as functions of the semiconductor band gap Δ_0, at different doping levels ε for $T = 0\,K$ and 2D constant density of states. Δ_m is the superconducting order parameter for the metallic ($\Delta_0 = 0$) case, Eq. (5). The dashed line is the conduction band edge E_c. When μ crosses below E_c, a crossover from BCS to BEC occurs.

Particle conservation in the doped semiconductor implies that the number of particles does not change as superconductivity sets in. Therefore, we need to ensure the equality between the number of particles in the normal and in the superconducting state: For an n-doped semiconductor, electrons are released into the conduction band by donor atoms. We model this by adding an extra number of electrons δN, which for a constant density of states in the conduction band can be written as $\delta N = 2\rho\varepsilon$. Here, $\varepsilon = \varepsilon_F - \Delta_0$ is the Fermi energy measured from the conduction band edge Δ_0.

$$\underbrace{2\rho\varepsilon}_{\delta N} + 2\rho\int_{-D}^{-\Delta_0} d\xi_k = \left(\int_{-D}^{-\Delta_0} + \int_{\Delta_0}^{D}\right) d\xi_k \left(1 - \frac{\xi_k - \mu}{E(\xi_k)}\right). \tag{13}$$

Here, $2D$ represents the total bandwidth of the semiconductor. For large $D + \mu \gg \Delta$ and $D - \mu \gg \Delta$, integration gives

$$2\varepsilon = 2\mu - \sqrt{(\Delta_0 + \mu)^2 + \Delta^2} + \sqrt{(\Delta_0 - \mu)^2 + \Delta^2}. \tag{14}$$

Eqs. (12) and (14) are the set of equations that describe the BCS superconducting state of semiconductors with constant density of states.

By numerically solving these equations we obtain plots for the superconducting order parameter Δ, Fig.3 (top) and the chemical potential μ Fig.3 (bottom) as functions of the semiconductor gap Δ_0. We thereby reproduce the results of Ref.[12]: in the undoped semiconductor there is a sharp superconductor-insulator transition at a critical Δ_{0c}, which occurs at half of the superconducting order parameter in a metallic superconductor, $\Delta_{0c} = \Delta_m/2$. Here Δ_m parametrizes the strength of the attractive interaction via Eq. (11). We note that this result holds in the limit of $\omega_D \gg \Delta_0$ only, where the energy range of attraction extends beyond the Energy gap Δ_0. In the opposite limit, the undoped system would remain in the insulator phase. At finite doping, the pairing amplitude Δ is finite for any value of the semiconducting gap Δ_0, since there are always charge carriers present, which can be paired for any value of Δ_0.

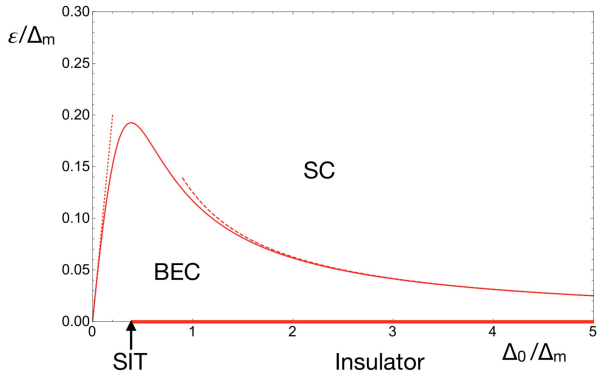

FIG. 4: BCS-BEC crossover diagram: doping parameter ε versus semiconductor band gap Δ_0 in units of Δ_m, as obtained by the crossover condition $\mu = \Delta_0$ for 2D DOS.

As mentioned above, there is a crossover to BEC at low concentration of charge carriers. This can be seen by the fact that as the paring sets in, the chemical potential μ drops below the conduction band edge even when it has been in the conduction band before, see Fig.3(bottom). We obtain the correlation length for the 2D density of states for $D \gg \Delta_0$,

$$\xi^2 = \frac{1}{4m\Delta} h(s = \frac{\mu}{\Delta}, t = \frac{\Delta_0}{\Delta}), \tag{15}$$

where

$$h(s,t) = (\pi - \arctan(t-s) - \arctan(t+s))^{-1} \langle 2 - \pi t + \sum_{\alpha=\pm 1} ((t - \alpha s)\arctan(t-\alpha s) + \frac{1}{(t-\alpha s)^2 + 1}) \rangle. \tag{16}$$

For $\mu > \Delta_0$ we recover the BCS coherence length ξ given by $\xi^2 = \frac{\mu - \Delta_0}{4m\Delta^2}$.[27] When the chemical potential is at the band edge $\mu = \Delta_0$, we find $\xi^2 = 1/(\pi m\Delta)$, which is the size of a single bound electron pair with pairing energy Δ. For the undoped semiconductor with symmetric bands, $\mu = 0$, the coherence length is given by $\xi^2 = 1/(3m\Delta_0)$ for $\Delta \to 0$, which coincides with the size of a single bound electron pair with binding energy Δ_0. For $|\mu| < \Delta_0$ and $\Delta \to 0$ one finds $\xi^2 = 1/(3m\Delta_0)(\Delta_0^2 + \mu^2)/(\Delta_0^2 - \mu^2)$. We note that while this defines the smallest size of the bound pair in this simple two-band model with band gap $2\Delta_0$, the actual size of the bound

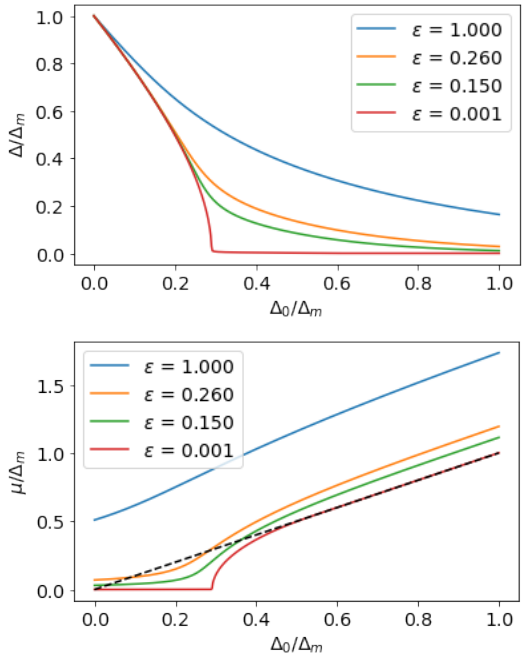

FIG. 5: Top: superconducting order parameter Δ. Bottom: chemical potential μ as function of semiconductor band gap Δ_0, at different doping levels ε for $T = 0\,K$ for 3D density of states. Δ_m is the superconducting order parameter for the metallic ($\Delta_0 = 0$) case, Eq. (5). The dashed line is the position of the conduction band edge E_c. When μ crosses below E_c, a crossover from BCS to BEC occurs.

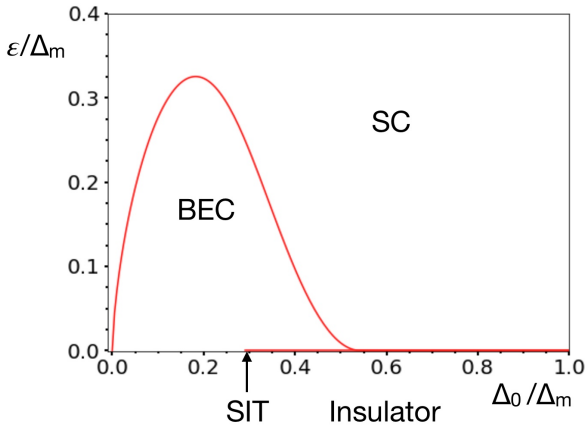

FIG. 6: BCS-BEC Crossover diagram: doping parameter ε versus semiconductor band gap Δ_0 in units of Δ_m as obtained by the crossover condition $\mu = \Delta_0$ for 3D DOS.

electron pair is modified by the fact that the states in the tails of the band of a doped semiconductor are localized with a finite localization length L_c, which in the dilute dopant limit becomes the effective Bohr radius of the ground state of the dopant levels. Thus, as the doping is reduced there occurs a metal-insulator transition to Anderson localized states, which has to be implemented in the pairing theory to obtain a more realistic description of the BCS-BES crossover and may result in a localization transition to localized bosons.[29]

We conclude that there is a crossover from superconductivity to dilute bound electron pairs when the chemical potential is at one of the band edges, $\mu = \pm\Delta_0$. Inserting that condition into Eqs. (12), (14) we find $\varepsilon = \Delta_0 + \Delta/2 - \sqrt{\Delta_0^2 + \Delta^2/4}$, where Δ is the positive solution of the quartic equation $\Delta^4/\Delta_m^4 + 4\Delta\Delta_0/\Delta_m^2 - 1 = 0$. Thereby, the quantum phase diagram in the parameter space of doping ε versus Δ_0, see Fig.4 showing a parameter regime where Bose-Einstein condensation occurs below a critical temperature T_c. This diagram has already been obtained for the two-band model with a 2D density of states in Ref..[12] For $\Delta_0 \gg \Delta$, one obtains that the BCS-BEC crossover occurs for $\varepsilon/\Delta_m = 1/(8\Delta_0/\Delta_m)$ (dashed line in Fig. 4). For $\Delta_0 \ll \Delta$, one obtains that the BCS-BEC crossover occurs for $\varepsilon/\Delta_m = \Delta_0/\Delta_m$ (dotted line in Fig.4).

B. Two-band model with 3D DOS

Next, we consider a density of states (DOS) which is more realistic for 3-dimensional semiconductors, shown in Fig. 1(right) (green): the DOS has a square-root dependence on the energy, in the conduction band, $\rho(\xi_k) = \rho_{0c}\sqrt{\xi_k - E_c}$, for $E_c < \xi_k < D$, whereas in the valence band $\rho(\xi_k) = \rho_{0v}\sqrt{-\xi_k + E_v}$, for $-D < \xi_k < E_v$, and $\rho(\xi_k) = 0$ in the band gap for $E_v < \xi_k < E_c$. Here, $\rho_{0c/v} = \sqrt{2m_{c/v}^3}/(\hbar^3\pi^2)$, where $m_{c/v}$ is the effective mass in the conduction/valence band, respectively. We assume $m_c = m_v$ in the following. As outlined in the Appendix the BCS equation yields then, assuming that ω_D is a large energy scale, Eq. A4 and the particle conservation yields Eqs. A3. This defines the set of equations that model the three-dimensional BCS superconducting semiconductors yielding the order parameter Δ and the chemical potential μ. We solve these equations numerically to obtain the superconducting order parameter Δ, Fig. 5(top), and chemical potential μ, Fig. 5(bottom) as functions of the semiconductor gap Δ_0, the attractive interaction U via $\Delta_m = 2\omega_D \exp(-1/(\rho U))$, and the doping parameter ε/Δ_m. Without doping, $\varepsilon = 0$, the superconducting order parameter Δ drops to zero when the semiconductor gap reaches the critical value $\Delta_{0c} = 0.29\Delta_m$. Thus, this superconductor-insulator transition occurs already at a smaller semiconducting band gap, than for the step function DOS, as expected, since the density of states is smaller when approaching the band edges compared to the 2D case, and thus less quasiparticles are available to pair and participate in the condensate. For finite ω_D, there would only be a superconducting phase when $\omega_D > \Delta_0$. For finite doping ε, the order parameter Δ persists for all values of the semiconductor gap Δ_0, but is for the same values of (Δ_0, ε) substantially smaller than for the step function DOS. As discussed in the previous section, the condition $\mu = \pm\Delta_0$ gives the BCS-BEC crossover line in parameter space spanned by the doping parameter ε and the semiconductor gap Δ_0. In Fig. 6 we plot the resulting phase diagram

as obtained by a numerical solution of the above equations for the 3D DOS for $\mu = \Delta_0$. Remarkably, we find that for large semiconductor band gaps $\Delta_0 > \Delta_0^* = 0.5\Delta_m$, there is no solution with $\mu = \Delta_0$ for finite doping $\varepsilon > 0$, within the numerical accuracy of at least 10^{-4}, so that there exists no BEC, but rather a direct transition to a BCS superconductivity phase as shown in Fig. 6.

III. SPATIAL VARIATION ALONG A SUPERCONDUCTING P-N JUNCTION

Having derived the superconducting order parameter Δ and chemical potential μ as functions of the semiconductor gap Δ_0 and the doping level ε, we can study the effect of pairing on the properties of p-n junctions in the presence of an attractive interaction U. For doping levels $\varepsilon_{n,p}$ the potential drop across a conventional p-n junction is given by

$$e\,\Delta\phi = \varepsilon_n + \varepsilon_p + 2\Delta_0. \tag{17}$$

The charge density drops in the depletion region which has on the n-side a width d_n and on the p-side the depletion width d_p. Using Poisson's equation, $\frac{d^2\phi}{dx^2} = \varrho(x)/\epsilon$, where $\varrho(x)$ is the charge density and ϵ is the dielectric constant, one finds in the depletion approximation, which assumes, when solving the Poisson equation, that there are no charge carriers in the depletion region,

$$-e\phi(x) = \frac{e\Delta\phi}{N_D + N_A} \cdot \begin{cases} -N_A, x > d_n, \\ -N_A(1 - (\frac{x}{d_n} - 1)^2), d_n > x > 0, \\ N_D(1 - (\frac{x}{d_p} + 1)^2), -d_p < x < 0, \\ N_D, x < -d_p. \end{cases} \tag{18}$$

Here, the depletion lengths in the n, p regions are respectively given by $d_{n/p} = (N_{A/D}/N_{D/A}\epsilon\Delta\phi/(2\pi e(N_D + N_A)))^{1/2}$, where ϵ is the bulk dielectric constant of the semiconductor. For a given energy gap of the semiconductor Δ_0, we thus obtain the spatial variation of the conduction and valence band edges across the p-n junction,

$$E_C(x) = -e\phi(x) + \Delta_0, E_V(x) = -e\phi(x) - \Delta_0, \tag{19}$$

as plotted in Fig. 7 (black lines). The electrochemical potential is given by $\mu_{em}(x) = \mu + e\phi(x)$. For simplicity we assume that both, the n- and p-sides are equally doped, $\varepsilon_n = \varepsilon_p = \varepsilon$, $N_A = N_D$, $d = d_n = d_p = d = (\epsilon\Delta\phi/(4\pi eN))^{1/2}$. As we consider the p-n junction without an external bias, the chemical potential μ remains independent of the position x across the junction, $\mu = 0$ (blue line in Fig. 7).

Turning on superconductivity takes charge carriers into the condensate, changing the electrochemical energy on both sides of the junction by an amount which equals the superconducting binding energy. Thereby, the potential energy drops across the p-n junction in the presence of superconductivity by an amount given by

$$\begin{aligned} e\,\Delta\phi_S &= e\phi_S(x \ll -d_p) - e\phi_S(x \gg d_n) \\ &= 2\mu_{em}(\Delta_0, \varepsilon, \Delta_m), \end{aligned} \tag{20}$$

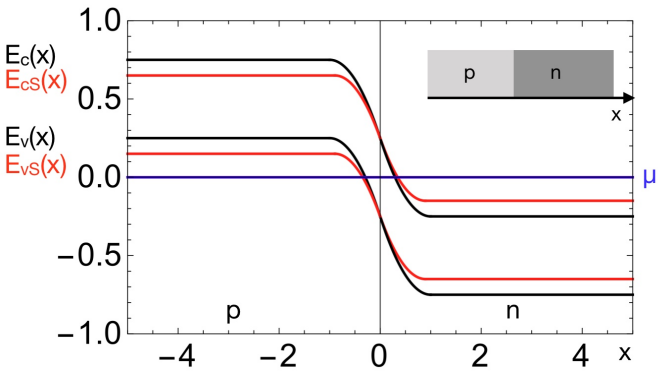

FIG. 7: Energy Band diagram of p-n junction with spatial variation of band edges $E_C(x), E_V(x)$ (black). Superconductivity caused by the attractive interaction shifts the band edges to $E_{CS}(x), E_{VS}(x)$ (red). The chemical potential remains constant without external bias (blue). Inset: geometry of the p-n junction.

where the parameters $\Delta_0, \varepsilon, \Delta_m$ are the semiconductor band gap, the doping level and the superconducting order parameter in the metallic limit, as defined above.

This change of the potential drop changes the spatial dependence of the potential $\phi_S(x)$, accordingly, resulting in the new spatial variation of the band edges,

$$E_{CS}(x) = -e\phi_S(x) + \Delta_0, E_{VS}(x) = -e\phi_S(x) - \Delta_0. \tag{21}$$

In depletion approximation this yields

$$-e\phi(x) = \frac{e\Delta\phi^S}{2} \cdot \begin{cases} -1, x > d^s, \\ -1 + (\frac{x}{d^s} - 1)^2, d^s > x > 0, \\ 1 - (\frac{x}{d^s} + 1)^2, -d^s < x < 0, \\ 1, x < -d^s, \end{cases} \tag{22}$$

with the depletion width reduced to $d^s = (\epsilon\Delta\phi^s/(4\pi eN))^{1/2}$.

The spatial variation of $\Delta(x)$ at junctions can be derived from the Gorkov equations,[31] or equivalently from the Bogoliubov-de Gennes equations,[32].[33] For Josephson contacts, such as junctions of superconductors with an insulating oxide layer in between, it was found that $\Delta(x)$ varies in close vicinity of the junction on length scales of the order of the insulator thickness, as imposed by the drop of the charge density in the oxide layer. Further away from the junction, however, $\Delta(x)$ varies on length scales of the order of the bulk coherence length ξ,[32],[33] since the variations on shorter length scales in in the bulk superconductor energetically suppressed by long range order. Thus, when the coherence length is larger than the depletion length, $\xi = v_F/\Delta > d$, we can assume that the spatial variation of $\Delta(x)$ at the p-n junction is dictated by the electrostatics at the junction, and thereby the reduced charge carrier density as parameterised by the the electrochemical potential $\mu_{em}(x)$. While the chemical potential μ is constant in the p-n junction without external bias, the chemical potential entering in the pairing equation Eq. (12) for the 2D system,

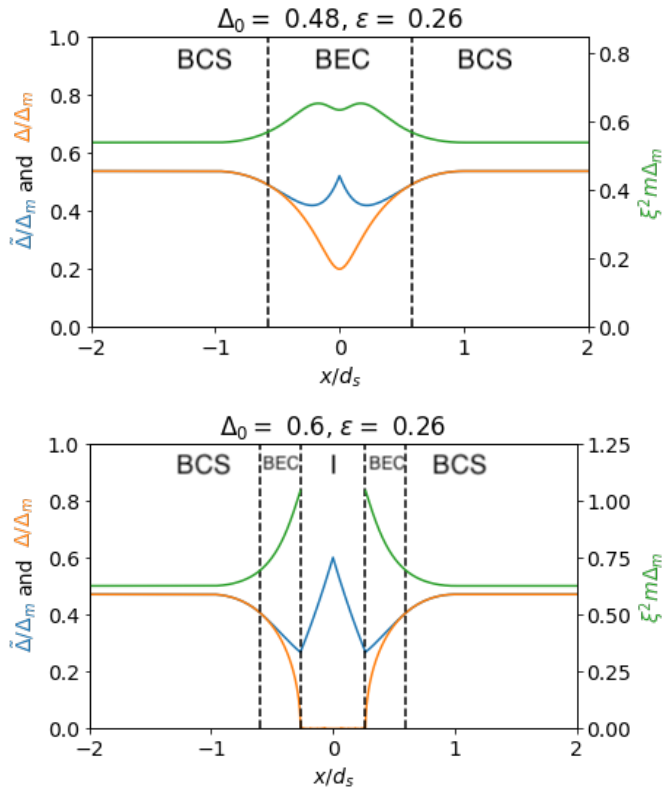

FIG. 8: Order parameter $\Delta(x)$, quasiparticle gap $\tilde{\Delta}(x)$, and the coherence length $\xi(x)$ across two types of 2D p-n junctions. (Top) BCS-BEC-BCS with semiconductor gap $\Delta_0 = 0.48\Delta_m$ and doping $\varepsilon = 0.26\Delta_m$. (Bottom) BCS-BEC-I-BEC-BCS with semiconductor gap $\Delta_0 = 0.6\Delta_m$ and doping $\varepsilon = 0.26\Delta_m$.

and in Eq. (A4) for the 3D system is rather the electrochemical potential $\mu_{em}(x)$ as measured relative to the middle of the semiconductor gap at the respective position x, which is for $\mu = 0$ in depletion approximation given by

$$\mu^s_{em}(x) = \mu_{em}(\Delta_0, \varepsilon, \Delta_m)) \cdot \begin{cases} 1, x > d^s, \\ 1 - (\frac{x}{d^s} - 1)^2, d^s > x > 0, \\ -1 + (\frac{x}{d^s} + 1)^2, -d^s < x < 0, \\ -1, x < -d^s, \end{cases} \tag{23}$$

Therefore, to get the spatial variation of $\Delta(x)$ on length scale d along the length of the p-n junction for different values of Δ_0 and ε, we can in a first, local density approximation, insert $\mu_{em}(x)$ as given by Eq. (23) into the pairing equation Eq. (12) for the 2D system, and in Eq. (A4) for the 3D system and solve for $\Delta(x)$ for every position x.

p-n junction of 2D systems. For the 2D system we find thereby two different kinds of superconducting p-n junctions when the bulk is in the BCS phase:

1. **BCS-BEC-BCS junction**: For $\Delta_0 < \Delta_m/2$ the order parameter $\Delta(x)$ decreases in the space charge region, but remains finite with a minimum in the middle of the pn-junction, as shown in Fig. 8 (Top). However, we find that even when the bulk system is in the BCS superconducting phase, there emerges a BEC layer at the pn-junction as the chemical potential moves into the band gap at the pn-junction. This BEC condensate extends throughout the pn-junction in a regime of width $d_{BEC} = 2d_s(1 - \sqrt{1 - \Delta_0/\mu_{\rm em}})$, as obtained by the condition $\mu_{\rm em}(x = \pm d_{BEC}/2) = \pm\Delta_0$. The quasiparticle excitation gap $\tilde{\Delta}(x)$ remains for the condition $\Delta_0 < \Delta_m/2$ finite throughout the pn-junction, decreasing first as the order parameter $\Delta(x)$ decreases, reaching a minimum and increasing again, as the chemical potential moves in the middle of the semiconductor band gap. Interestingly, the coherence length, which we calculate approximately using Eq. (15), in the BCS phase increases with the decrease of $\Delta(x)$, but converges to a finite value in the BEC phase, and decreases to a minimum, in the middle of the pn-junction.

2. **BCS-BEC-I-BEC-BCS junction**: For $\Delta_0 > \Delta_m/2$ the order parameter $\Delta(x)$ is found to decrease in the space charge region to 0 , as shown in Fig. 8 (Bottom), with a finite layer of an insulator phase in the middle of the junction. Thus, as the chemical potential moves into the band gap at the pn-junction, there is a BEC condensate at each of the two surfaces of the p-n junction, each of finite width $d_{BEC} = d_s((1 - \frac{\Delta_0}{\mu_{\rm em}}\sqrt{1 - \Delta_m^2/(4\Delta_0^2)})^{1/2} - (1 - \frac{\Delta_0}{\mu_{\rm em}})^{1/2})$, separated by an insulating layer, where $\Delta = 0$. The quasiparticle excitation gap $\tilde{\Delta}(x)$ remains finite throughout the pn-junction, decreasing first as the order parameter $\Delta(x)$ decreases, reaching a minimum at the boundary between the BEC and the insulator phase and increasing again in the insulator layer, as the chemical potential moves in the middle of the semiconductor band gap. Interestingly, the coherence length, as approximated with Eq. (15) which in the BCS phase increases with the decrease of $\Delta(x)$, converges to a finite value at the boundary between the BEC and the insulator phase, where the order parameter vanishes.

p-n junction of 3D systems. In the 3D systems we find, when the bulk is in the BCS phase, a BEC layer at the pn-junction occurs only for sufficiently small semiconductor gaps $\Delta_0 < \Delta_0^*$. Thus, we find in 3D three different kinds of superconducting p-n junctions, when the bulk is in the BCS phase:

1. **BCS-BEC-BCS junction**: For small semiconductor gaps $\Delta_0 < \Delta_{0c} == 0.29\Delta_m$ the order parameter $\Delta(x)$ decreases in the space charge region, but remains finite with a minimum in the middle of the pn-junction, as shown in Fig. 9 (Top). Thus, as the chemical potential moves into the band gap at the pn-junction, there appears a BEC condensate, where the chemical potential is outside of the band edges, which extends throughout the pn-junction in a regime of width d_{BEC}, as obtained by the condition $\mu_{\rm em}(x = \pm d_{BEC}/2) = \pm\Delta_0$. The quasiparticle excitation gap $\tilde{\Delta}(x)$ remains finite throughout the pn-junction, decreasing first as the order parameter $\Delta(x)$ decreases, reaching a minimum and increasing again, as the chemical potential moves into the middle of the semiconductor band gap.

2. **BCS-BEC-I-BEC-BCS junction**: For large semiconductor band gaps $\Delta_0 > \Delta_{0c} == 0.29\Delta_m$ the order parameter $\Delta(x)$ decreases in the space charge region to 0 , as shown in Fig. 9 (Center), with a finite layer of an insulator phase in the middle of the junction. Thus, as the chemical potential

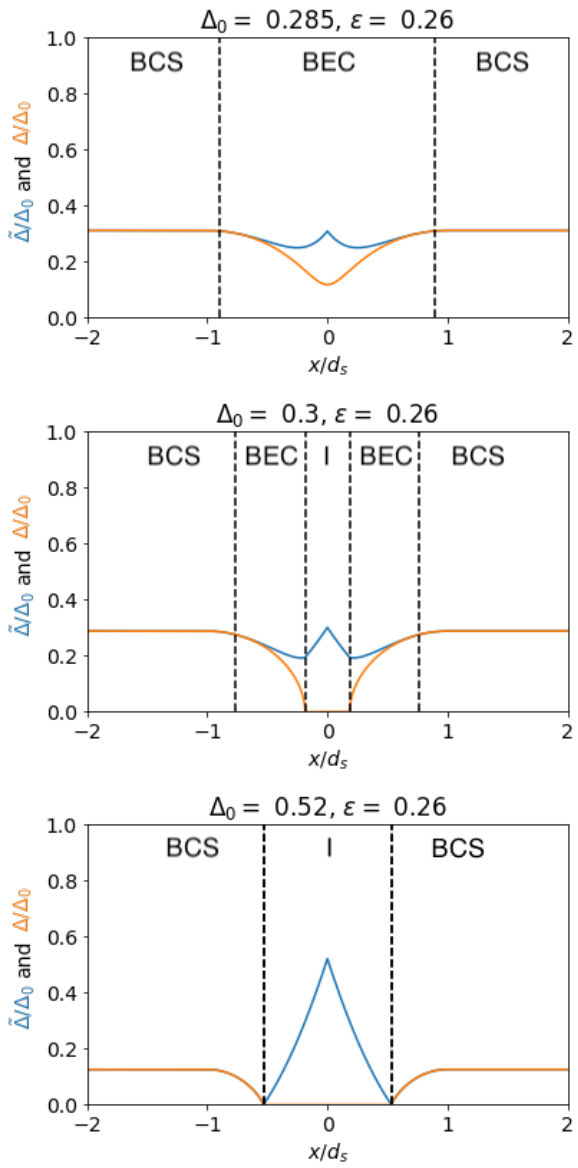

FIG. 9: The spatial variation of the order parameter $\Delta(x)$ and the quasiparticle gap $\tilde{\Delta}(x)$ across the 3D p-n junction. (Top) BCS-BEC-BCS junction with semiconductor gap $\Delta_0 = 0.285\Delta_m < \Delta_{0c}$ and doping $\varepsilon = 0.26\Delta_m$. (Center) BCS-BEC-I-BEC-BCS junction with semiconductor gap $\Delta_0 = 0.3\Delta_m > \Delta_{0c}$ and doping $\varepsilon = 0.26\Delta_m$. (Bottom) BCS-I-BCS junction with semiconductor gap $\Delta_0 = 0.52\Delta_m$ and doping $\varepsilon = 0.26\Delta_m$, showing the appearance of gapless quasiparticle excitations at the boundary between the BCS and the insulator phase.

moves into the band gap at the pn-junction, there is a BEC condensate at each of the two surfaces of the p-n junction, each of finite width d_{BEC}, separated by an insulating layer, where $\Delta = 0$. The quasiparticle excitation gap $\tilde{\Delta}(x)$ remains finite throughout the pn-junction, decreasing first as the order parameter $\Delta(x)$ decreases, reaching a minimum at the boundary between the BEC and the insulator phase and increasing again in the insulator layer, as the chemical potential moves into the middle of the semiconductor band gap.

3. **BCS-I-BCS junction**: For still larger semiconductor band gaps, $\Delta_0 > \Delta_0^* == 0.5\Delta_m$, there is no BEC layer anymore, the order parameter $\Delta(x)$ decreases to zero as the chemical potential reaches the band edge, as shown in Fig. 9 (Bottom), reaching directly an insulator phase as the chemical potential moves into the band gap at the pn-junction. Remarkably, the quasiparticle excitation gap $\tilde{\Delta}(x)$ vanishes at the boundary of the space charge region, decreasing first to zero as the order parameter $\Delta(x)$ decreases to zero, and increasing again in the insulator layer, as the chemical potential moves into the middle of the semiconductor band gap. Thus, there appear gapless quasiparticle excitations at the boundary to the space charge region.

IV. CONCLUSIONS AND DISCUSSION

Thus, we have shown that in superconducting pn-junctions there can appear layers of BEC condensates even when the bulk is in the BCS state. This opens the possibility to create layers of BEC and study their properties in the well controlled setting of doped semiconductors, where the doping level can be varied to change and control the thickness of BEC and insulator layers. The BEC condensate can be detected by scanning tunneling microscopy, where instead of the sharp coherence peaks in the BCS phase, a maximum in the tunneling density of states in the band which is closest to the chemical potential, is expected, as plotted in Fig. 3 (Bottom). Also, the fact that the quasiparticle excitation gap remains finite throughout the pn-junction when there is a BEC layer, while there are gapless excitations in a conventional BCS-I-BCS junction, might be amenable to experimental detection.

Moreover, attaching sufficiently small leads in lateral direction, the superconducting pn-junction may enable one to study the transport properties of the BEC layers directly.

As qualitatively outlined in Ref.23, the superconductor critical current I_c is expected to be still dominated by the bulk superconducting order parameter Δ and the normal small voltage resistance of the pn-junction R_n, as in a conventional Josephson contact, yielding for identical Δ on both sides of the junction $I_c R_n = \pi\Delta/(2e)$. The presence of a BEC layer might modify that product due to the spatial variation of the order parameter, and the quasiparticle exciation gap, see Figs. 8,9. We will leave the derivation as a task for further studies.

For a conventional semiconductor with $\epsilon = 10$, $\Delta\Phi = 1V$ and $N_D = N_A = 10^{18} cm^{-3}$, the depletion width is $d \approx 50nm$,[23] whereas in p-n junctions of cuprate semiconductors $\Delta\Phi$ can be several volts, $N_D = N_A = 5. \times 10^{21} cm^{-3}$, yielding only $d \approx 1nm$ which is the same order as the thickness of oxide barriers in typical Josephson junctions. Indeed, cuprate semiconductors with a superconducting phase for both hole and electron doping have been found, see Ref.30 for a review, which may therefore be realisations of homogeneous p-n junctions, where we can expect BEC layers of the thickness of the order of $d_{BEC} \approx 1nm$.

The theory can be extended to hetero-junctions with two different host materials with different band gaps on the n- and

p- doped side of the junctions, resulting in band discontinuities at the junction to study what effect this has on the existence of a BEC layer.

The $I(V)$ characteristics of superconducting pn junctions has been discussed qualitatively in Ref.23. We leave it for future work to extend our theory to include a potential difference and thereby allow a quantitative derivation of current voltage characteristics, and to study what consequence BEC-layers have for the I(V)-characteristics.

Recently, Josephson junctions in the BCS-BEC crossover range have been reviewed in Ref.33 by solving the Bogoliubov-de-Gennes equations for this problem. These authors did not discuss the appearance of a BEC layer at the junction when the bulk is in the BCS phase. However, we expect, that, since the carrier concentration is reduced in the vicinity of an oxide layer, a BEC layer may also appear at such BCS- Josephson junctions with an oxide layer, a question we leave for future research.

An extension of the Bogoliubov-de-Gennes equations,[32][33] to the 2-band model and its application to the superconducting p-n junctions will lead also further insights into the spatial variation of the order parameter, when solved self consistently with the Poisson equation. This calculation, where the condensation amplitude as well as the charge redistribution are self-consistently computed can be performed within the tight binding framework.[34–36] In particular, one can expect deviations from our result for the spatial change of $\Delta(x)$ on length scales of the order of the bulk coherence length ξ. Also, additional discrete states might appear as solutions of the Bogoliubov-de-Gennes equations at the junction, similar to the Andreev bound states found in Josephson junctions.[33] This raises interesting questions for future research, as the change from electron like to hole like charge carriers across the junction challenges the conventional interpretation of Andreev bound states.

In our study we have assumed zero temperature $T = 0K$, and it remains to be extended to finite temperatures T. Furthermore, while our study employs the mean field approximation of the many body physics, the effect of fluctuations of the order parameter amplitude and phase need to be included to get a better understanding of the stability of the long range order at finite temperature and in the thin film, 2D limit,[38],[12],[37]

The disorder introduced by the dopants will furthermore lead to Anderson localization of charge carriers and accordingly may result in a layer of disorder localized Bosons at the p-n junction, reducing the thickness of the extended BEC layer. These issues will be subject for future research.

Acknowledgments

S.K. gratefully acknowledges support from DFG KE-807/22-1. This work was supported by the US Department of Energy under grant number DE-FG03-01ER45908. The numerical computations were carried out on the University of Southern California High Performance Supercomputer Cluster.

Appendix A: 3D 2-band model

Following an approach similar to Eagles,[11] who solved the BCS equation and particle conservation equation for a single-band semiconductor, we rearrange the particle conservation equation Eq. 1 of the two-band model to get

$$\frac{2}{3}\left(\frac{\varepsilon}{\Delta}\right)^{\frac{3}{2}} = Q(\lambda_1) - Q(\lambda_2), \tag{A1}$$

where $Q(\lambda_i) = \int_0^\infty x^2 dx (1 - (x^2 - \lambda_i)/\sqrt{1 + (x^2 - \lambda_i)^2})$for $i = 1, 2$. with $\lambda_1 \equiv (\mu - \Delta_0)/\Delta$, and $\lambda_2 \equiv (-\Delta_0 - \mu)/\Delta$. Here, we changed the integration parameters to $x^2 = (\xi - \Delta_0)/\Delta$ for $i = 1$ and $x^2 = (\xi + \Delta_0)/\Delta$ for $i = 2$. We approximated $D/\Delta \to \infty$. As in the 2D limit, we assume that ω_D is a large energy scale, for simplicity. This means that we assume that the electron-electron interaction is attractive in both bands. Therefore, we can set $\omega_D = D$ so that the BCS self-consistency equation simplifies to

$$1 \simeq \rho_0 U \Delta^{\frac{1}{2}} \left[P(\lambda_1) + P(\lambda_2) + \sqrt{\frac{4\omega}{\Delta}} \right], \tag{A2}$$

where $P(\lambda_i) = \int_0^\infty dx (x^2/\sqrt{1 + (x^2 - \lambda_i)^2} - 1)$, $i = 1, 2$. We follow the approach by Pistolesi[26] to rewrite Eqs. A1 and A2 in terms of elliptical integrals and obtain for the equation ensuring particle conservation

$$\frac{2}{3}\left(\frac{\varepsilon}{\Delta}\right)^{\frac{3}{2}} = \sum_{i=1,2} \sigma_i \lambda_i \left(1 + \lambda_i^2\right)^{\frac{1}{4}} E\left(\frac{\pi}{2}, k_i\right) + \sum_{i=1,2} \sigma_i \frac{(1 + \lambda_i^2)^{1/4}}{2(\lambda_i + \sqrt{1 + \lambda_i^2})} F(\frac{\pi}{2}, k_i), \tag{A3}$$

where $\sigma_1 = 1$, $\sigma_2 = -1$ and $k_i^2 = \frac{\sqrt{1+\lambda_i^2}+\lambda_i}{2\sqrt{(1+\lambda_i^2)}}$ for $i = 1, 2$. Here, $F(\varphi, k)$ are $E(\varphi, k)$ the incomplete elliptic integral of the first and second kind, respectively. The pairing equation becomes

$$1 = 2\rho_0 U \sqrt{\Delta} \sum_{i=1,2} \left[-\left(1 + \lambda_i^2\right)^{\frac{1}{4}} E\left(\frac{\pi}{2}, k_i\right) + \frac{F\left(\frac{\pi}{2}, k_i\right)}{2(1 + \lambda_i^2)^{\frac{1}{4}}} \left(\lambda_i + \frac{1}{\sqrt{1 + \lambda_i^2} + \lambda_i} \right) + \sqrt{\frac{\omega_D}{\Delta}} \right]. \tag{A4}$$

We denote the metallic limit by $\Delta(\Delta_0 = 0) = \Delta_m$, as defined by Eq. (A4), when substituting there $\Delta_0 = 0$, Δ by Δ_m and λ_i by $\widetilde{\lambda}_1 = \lambda_i|_{\Delta_0=0,\Delta=\Delta_m}$ and $\widetilde{k}_i^2 = \frac{\sqrt{1+\widetilde{\lambda}_i^2}+\widetilde{\lambda}_i}{2\sqrt{1+\widetilde{\lambda}_i^2}}$ for $i = 1, 2$. Since we assume that the local attraction U between the fermions does not depend on Δ_0, we can equate the right hand side of Eq. A4 with finite Δ_0 to the one obtained in the metallic limit. This equation gives together with Eqs. A3 the new set of equations that model the three-dimensional BCS superconducting semiconductors.

[1] M. L. Cohen, Rev. Mod. Phys. 36, 240 (1964)

[2] W. Hanke and M. J. Kelly, Phys. Rev. Lett. 45, 1203 (1980)

[3] X. Lin, Z. Zhu, B. Fauqu, and K. Behnia, Phys. Rev. **X 3**, 021002 (2013).

[4] E. A. Ekimov, V. A. Sidorov, E. D. Bauer, N. N. Melnik, N. J. Curro, J. D. Thompson, and S. M. Stishov, Nature 428, 542 (2004).

[5] X. Blase, Ch. Adessi, and D. Connetable, Phys. Rev. Lett. 93, 237004 (2004).

[6] E. Bustarret, J. Kacmarcik, C. Marcenat, E. Gheeraert, C. Cytermann, J. Marcus, and T. Klein, Phys. Rev. Lett. 93, 237005 (2004).

[7] E. Bustarret, C. Marcenat, P. Achatz, P J. Kacmarcik, F. Lévy, A. Huxley, L. Ortéga, E. Bourgeois, X. Blase, D. Débarre and J. Boulmer. Nature **444**, 465 (2006); R. Skrotzki, J. Fiedler, T. Herrmannsdörfer, V. Heera, M. Voelskow, Mücklich, B. Schmidt, W. Skorupa, G. Gobsch, M. Helmand J. Wosnitza, Appl. Phys. Lett. **97**, 192505 (2010).

[8] L. N. Cooper, Phys. Rev. 104, 1189 (1956)

[9] J. Bardeen, L. N. Cooper, and J. R. Schrieffer, Phys. Rev. 106, 162 (1957)

[10] J. Bardeen, L. N. Cooper, and J. R. Schrieffer, Phys. Rev. 108, 1175 (1957)

[11] D. M. Eagles, Phys. Rev. 186, 456 (1969).

[12] P. Nozires and F. Pistolesi, Eur. Phys. J. B 10, 649 (1999).

[13] A. V. Chubukov, I. Eremin, D. V.Efremov, Phys. Rev. B 93, 174516 (2016).

[14] Y. L. Loh, M. Randeria, N. Trivedi, C.-C. Chang, R. Scalettar, Phys. Rev. **X 6**, 021029 (2016).

[15] Y. Yerin, H. Tajima, P. Pieri, A. Perali, Phys. Rev. **B 100**, 104528 (2019).

[16] A. J. Leggett, Diatomic molecules and Cooper pairs, in Modern Trends in the Theory of Condensed Matter, ed. by A. Peralski and Przystawa, Springer, Berlin (1980).

[17] C. A. Regal, M. Greiner, D. S. Jin, Phys. Rev. Lett. **92**, 040403 (2004).

[18] M. W. Zwierlein, C. A. Stan, C. H. Schunck, S. M. F. Raupach, A. J. Kerman, W. Ketterle, Phys. Rev. Lett. 2004 92, 120403.

[19] S. Rinott, K. B. Chashka, A. Ribak, E. D. L. Rienks, A. Taleb-Ibrahimi, P. L. Fevre, F. Bertran, M. Randeria, and A. Kanigel. Science Advances, 3(4) (2017).

[20] Y. Nakagawa, Y. Saito, T. Nojima, K. Inumaru, S. Yamanaka, Y. Kasahara, and Y. Iwasa. Phys. Rev. B, 98:064512 (2018).

[21] Y. Cao, V. Fatemi, S. Fang, K. Watanabe, T. Taniguchi, E. Kaxiras, and P. Jarillo-Herrero, Nature (London) 556, 43 (2018).

[22] I. Takeuchi, S. N. Mao, X. X. Xi, K. Petersen, C. L. Lobb, and T. Venkatesan, Appl. Phys. Lett. 67, 2872 (1995).

[23] J. Mannhart, A. Kleinsasser, J. Ströbel and A. Baratoff, Physica **C 216**, 401 (1993).

[24] X. Zhang, S. Saha, N. P. Butch, K. Kirshenbaum, J. Paglione, and R. L. Greene, Appl. Phys. Lett. 95, 062510 (2009).

[25] C. Wu, M.-J. Wang, M.-K. Wu, Physica **C 460 - 462**, 424 (2007).

[26] M. Marini, F. Pistolesi, and G. C. Strinati, Eur. Phys. J. B 1, 151 (1998)

[27] F. Pistolesi, and G. C. Strinati, Phys. Rev. B **49**, 6356 (1994).

[28] J. R. Schrieffer, *Theory of Superconductivity* , Perseus Books (1999).

[29] A.Ghosal,M.RanderiaandN.Trivedi,Phys.Rev.Lett. **81**, 3940 (1998); A. Ghosal, M. Randeria and N. Trivedi, Phys. Rev. B 63, 020505(2000); K. Bouadim, Y. L. Loh, M. Randeria and N. Trivedi, Nature Physics 7 (2011); M. V. Feigelman, L. B. Ioffe, V. E. Kravtsov and E. A. Yuzbashyan, Phys. Rev. Lett. **98**, 027001(2007); M. Feigelman, L. Ioffe, V. Kravtsov and E. Cuevas, Annals of Physics **365**, 1368 (2010); I. Burmistrov, I. Gornyi and A. Mirlin, Phys. Rev. Lett. **108**, 017002 (2012); A. M. Finkelstein, Physica B **197**, 636 (1994); B. Sacepe, T. Dubouchet, C. Chapelier, M. Sanquer, M. Ovadia, D. Shahar, M. Feigelman and L. Ioffe, Nat. Phys. **7**, 239(2011).

[30] M. R. Norman and C Pépin, Rep. Prog. Phys. **66**, 1547 (2003).

[31] A. I. Larkin, Yu. N. Ovchinnikov and M. A. Fedorov, J. Exp. Theor. Phys. **51**, 683 (1966).

[32] P. G. De Gennes, Rev. Mod. Phys. **36**, 225 (1964).

[33] A. Spuntarelli, P. Pieri, G.C. Strinati, Physics Reports 488, 111 (2010).

[34] A. Ghosal, M. Randeria and N. Trivedi, Phys. Rev. B. **65**, 014501 (2001).

[35] A. Black-Shaffer, S. Doniach, Phys. Rev. B. **78**, 024504 (2008).

[36] G. Rai, S. Haas, A. Jagannathan, Phys. Rev. B. **100**, 165121 (2019).

[37] A. Larkin and A. Varlamov, *Theory of fluctuations in superconductors*, Oxford University Press, Oxford (2005).

[38] J.M. Kosterlitz and J. Thouless, J. Phys. C 6, 1181 (1973).